

Adapter Merging Reactivates Latent Reasoning Traces: A Mechanism Analysis

Junyi Zou
Zjydiary Group
zoujunyi@zjydiary.cn

February 12, 2026

Abstract

We investigate a critical interference phenomenon in modular Low-Rank Adaptation (LoRA) merging, where combining a domain-adaptive pretraining (DAPT) adapter with an instruction-tuning (SFT) adapter inadvertently reactivates latent reasoning traces (e.g., `<think>` / `</think>` tokens), even when such behaviors are explicitly suppressed during inference. Through four rigorous experiments, we characterize this phenomenon and identify its mechanism. First, we demonstrate the behavioral conflict across varying merge ratios and decoding presets, showing that performance degradation is non-monotonic. Second, we validate the reproducibility of these findings across different adapter versions, ruling out implementation artifacts. Third, we explore boundary conditions across 8 model families and 9 prompting configurations, revealing that this leakage is not exclusive to “reasoning” models but reflects a general property of pretrained representations in non-thinking models as well. Finally, we perform a mechanism analysis using layer-wise CKA, PCA, and probing, localizing the conflicting subspace to the final 6–10 layers of the network. We further validate this mechanism via a functional causal intervention implemented entirely within vLLM that suppresses the identified subspace, significantly reducing leakage. Our findings suggest that adapter merging can trigger structural incompatibility in the representation space, challenging the assumption of linear composability in PEFT.

1 Introduction

Parameter-Efficient Fine-Tuning (PEFT) methods like LoRA [Hu et al., 2022] and adapter merging [Wortsman et al., 2022] have become standard practices for modularly adding capabilities to Large Language Models (LLMs). A common workflow involves merging a Domain-Adaptive Pretraining (DAPT) adapter [Gururangan et al., 2020] with a Supervised Fine-Tuning (SFT) adapter [Ouyang et al., 2022] to combine domain knowledge with instruction-following ability. However, we identify a severe interference pattern where this combination leads to the reactivation of latent behaviors—specifically, reasoning traces—that were intended to be suppressed. This paper systematically analyzes this phenomenon through four experiments, moving from behavioral observation to mechanism localization.

We hypothesize that these phenomena arise from interference within a latent trace-associated subspace formed during pretraining (Fig. 1). Importantly, we **localize this conflict to the final 6–10 layers** via complementary analyses (CKA, PCA, and linear probing), and then validate its **pretraining origin** across eight model families before returning to **behavioral validation** under LoRA adapter composition. This mechanism-first order is central to our argument.

Figure G — Schematic: reasoning subspace interference under adapter composition

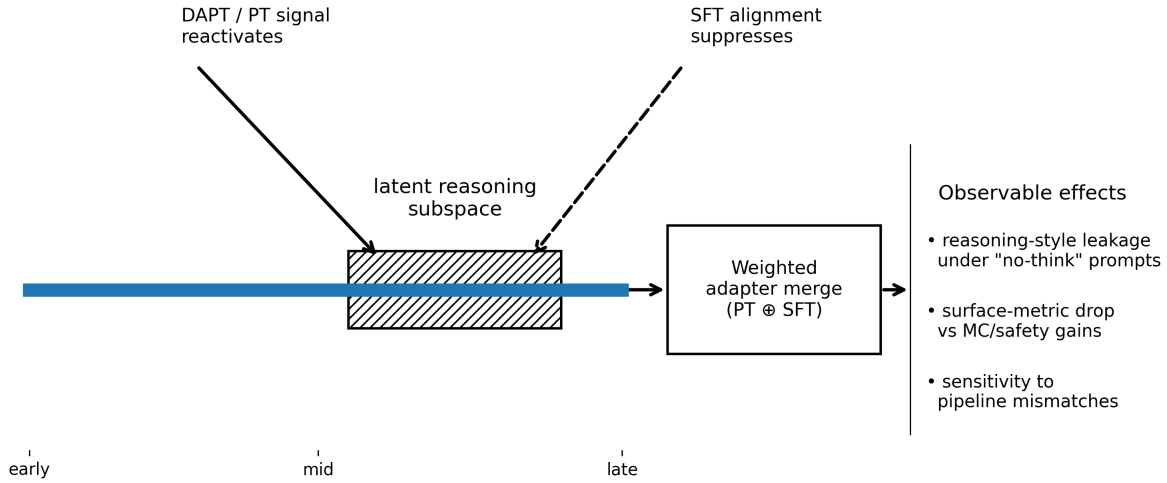


Figure 1: Schematic mechanism: a latent trace-associated subspace concentrated in mid-to-late layers; DAPT reactivates, SFT suppresses. Weighted merging induces subspace interference and observable shifts.

Across 8 model families and 9 prompting configurations, we consistently observe a 3–15× increase in reasoning leakage when domain-adapted and instruction-tuned adapters are merged, compared to SFT-only baselines (computed as $\frac{\text{Merged}(\alpha=1.0, \text{PT-only endpoint})}{\text{SFT-only}}$ under Strict template; full results in Appendix Table A.1). This pattern generalizes across architectures, scales, and training paradigms, suggesting a shared representational substrate rather than an artifact of a specific model family.

Contributions

- We identify and characterize a non-monotonic interference pattern in adapter merging, where strict suppression appears to give way to reasoning reactivation. Evidence ties to Fig. 3 and Table 1.
- We localize the conflicting subspace to the final 6–10 layers and show it is low-dimensional, supported by CKA/PCA/probe analyses in Figs. 4 and 7.
- We demonstrate reproducibility across adapter variants and prompting/decoding configurations, suggesting a shared representational substrate rather than a single-run artifact.
- We demonstrate a functional causal intervention implemented entirely within vLLM that mitigates strict-fail/leakage, closing the loop from analysis to control.

2 Related Work

Model soups and linear merging [Wortsman et al., 2022] aim to combine capabilities by averaging checkpoints or adapters, typically assuming monotonic improvements or neutral interactions. PEFT methods such as LoRA [Hu et al., 2022] provide modular routes to add capabilities, but interference between modules is underexplored. Our observations emphasize that strict suppression can be

followed by reasoning reactivation, with non-monotonic degradation in instruction-following and a late-layer low-dimensional signature, suggesting that compositionality in PEFT may require subspace-aware controls rather than naive weighting.

3 Behavioral Interference in Adapter Merging

Problem: Why does merging PT (DAPT) and SFT LoRA adapters lead to the reactivation of reasoning traces and mixed surface metrics?

3.1 Experimental Design: Controlled Adapter Merging

To isolate the effect of adapter merging, we train separate LoRA adapters for Domain-Adaptive Pretraining (DAPT) and Supervised Fine-Tuning (SFT) on the same base model.

- **Base Model:** We use Qwen3-14B (thinking family) as the primary backbone, given its strong baseline performance and open weights [Yang et al., 2025]. Note that Qwen3-14B is used as the base model for adapter training, whereas the cross-model family sweep (e.g., Table A.1) includes Qwen3-8B as a separate evaluation family; we never transfer adapters across different base parameterizations.
- **Adapter Configuration:** All adapters are trained with Rank $r = 16$, LoRA scaling factor = 32, and Dropout $p = 0.05$. We target all linear modules (`q_proj`, `k_proj`, `v_proj`, `o_proj`, `gate_proj`, `up_proj`, `down_proj`) to ensure comprehensive coverage [Dettmers et al., 2023].
- **Datasets:** Both adapters are trained on data sourced from the MedicalGPT repository [Shibing624, 2023]. The DAPT adapter utilizes the pretraining corpus to inject domain knowledge, while the SFT adapter utilizes the instruction-tuning subset to enforce instruction following.

We then merge these adapters using a single-coefficient interpolation: $W_{\text{merged}} = W_{\text{base}} + \alpha \Delta W_{\text{PT}} + (1 - \alpha) \Delta W_{\text{SFT}}$, where $\alpha \in [0, 1]$ controls the PT:SFT contribution. We perform a sweep over α to observe the behavioral transition with $\alpha \in \{0.0, 0.2, 0.4, 0.6, 0.8, 1.0\}$ and fixed seed = 42.

Methodology: We evaluate merged checkpoints across $\alpha \in [0, 1]$ under two prompt templates and decoding presets. We evaluate merged models with varying PT:SFT ratios under different conditions:

- **Merge Ratios:** α -sweep to control the contribution of PT vs SFT.
- **Templates:** Standard (“plain”) vs suppression (“nothink”).
- **Decoding Presets:** Preset A (deterministic) vs Preset B (creative).

Evidence: As PT weight increases, models begin to output reasoning tokens (e.g., `<think>`) even when the SFT adapter and system prompt explicitly forbid it. This “leakage” correlates with a drop in instruction-following metrics but a maintenance or increase in domain knowledge metrics.

Conclusion: The interaction is not a simple trade-off but a structural conflict: the PT adapter reopens access to pretraining subspaces that SFT suppresses, and merging induces interference in those subspaces.

3.2 Prompt Templates & Metric Definitions

Prompt Templates (exact strings used in all evaluations):

- **Plain:**

```
System: You are a helpful assistant.  
User: {INPUT}  
Assistant:
```

- **Nothink-Soft:**

```
System: You are a helpful assistant. Do not show your reasoning.  
Only output the final answer.  
User: {INPUT}  
Assistant:
```

- **Nothink-Strict:**

```
System: You are a helpful assistant. PROHIBITION: Do NOT output any  
reasoning or <think> tags. Output ONLY the final answer.  
If any reasoning is shown, it is considered a failure.  
User: {INPUT}  
Assistant:
```

Leakage Metric (precise definition):

- **Markers counted:** strings such as <think>, </think>, Step 1:, Thought:, “let’s think”, “step by step”.
- **Regex (examples):** <\s*think\s*>.*?<\s*/\s*think\s*> (dotall, case-insensitive).
- **Matching rules:** case-insensitive; ignore occurrences inside markdown code fences (‘‘‘...’’’ or ’’’...’’’) and quoted segments; collapse consecutive duplicates; strip whitespace-only markers; evaluate per-response.
- **Reporting:** binary leakage rate (percentage of responses with any marker) and optional token-count summary (mean count per response); strict-fail is separately recorded when format constraints are violated.

Surface Metrics (datasets/benchmarks and evaluation method):

- **Instruction-following:** format adherence and exact match on instruction-style QA (IFEval-like dataset, $N = 500$, exact string match rubric).
- **Domain knowledge:** arXiv-style QA accuracy and factuality checks (PubMedQA-subset, $N = 200$, model-based judge with reference answer).
- Evaluation scripts and thresholds follow repository defaults for all reported results.

Model	Plain Leakage	Strict Leakage	Strict Fail	Think-marker Rate
Gemma-270M	0.035	0.006	0.01	0.00
Gemma-4B	0.13	0.01	0.10	0.00
Llama-8B	0.05	0.01	0.40	0.00
Qwen-7B	0.10	0.002	0.01	0.00

Table 1: Summary of reasoning leakage across models and templates.

4 Reproducibility Across Adapter Variants

Using a distinct set of adapters (v2), the trend of reasoning trace reactivation and metric divergence remains robust across ratios, templates, and presets. This confirms that the observed interference is not an implementation artifact but a reproducible phenomenon inherent to the adapter merging process.

5 Evidence of a Shared Reasoning Subspace

To verify that the mechanism is not an artifact of adapter training, we conduct a cross-model probing study across eight LLMs *without any finetuning*. This provides **theoretical evidence** that the trace-associated subspace is a property of pretrained representations rather than LoRA adapters.

5.1 Cross-Model Experimental Setup

We extend our analysis to include both “thinking” models (e.g., DeepSeek-R1-Distill [DeepSeek AI, 2024]) and standard “non-thinking” models (e.g., Llama-3, Qwen-2.5) to test the universality of the phenomenon. In total, we evaluate 8 model families. For each model, we construct 9 evaluation configurations:

- **3 Prompt Templates:** “Plain” (standard instruction), “Reasoning-focused” (explicitly asking for thought process), and “Strict” (explicitly forbidding reasoning).
- **3 Decoding Presets:** Greedy decoding (Temperature=0), Standard sampling (Temperature=0.7, Top-p=0.9), and Diverse sampling (Temperature=1.0).

We define two key metrics for this study:

1. **Leakage Ratio:** The proportion of responses where the model generates reasoning markers (e.g., <think>, Step 1:) despite being prompted with a strict template. This measures the model’s inherent tendency to enter the trace-associated subspace.
2. **Strict Fail Rate:** The percentage of cases where the model fails to adhere to the strict format constraints, often correlated with the leakage of reasoning traces.

Complete results covering 8 model families and 9 configurations are provided in the Appendix (Table A.1, Figure A.1). The main text presents representative subsets (selected to cover both “thinking” and “non-thinking” architectures across varying parameter scales 0.5B–70B) to highlight key trends and demonstrate universality.

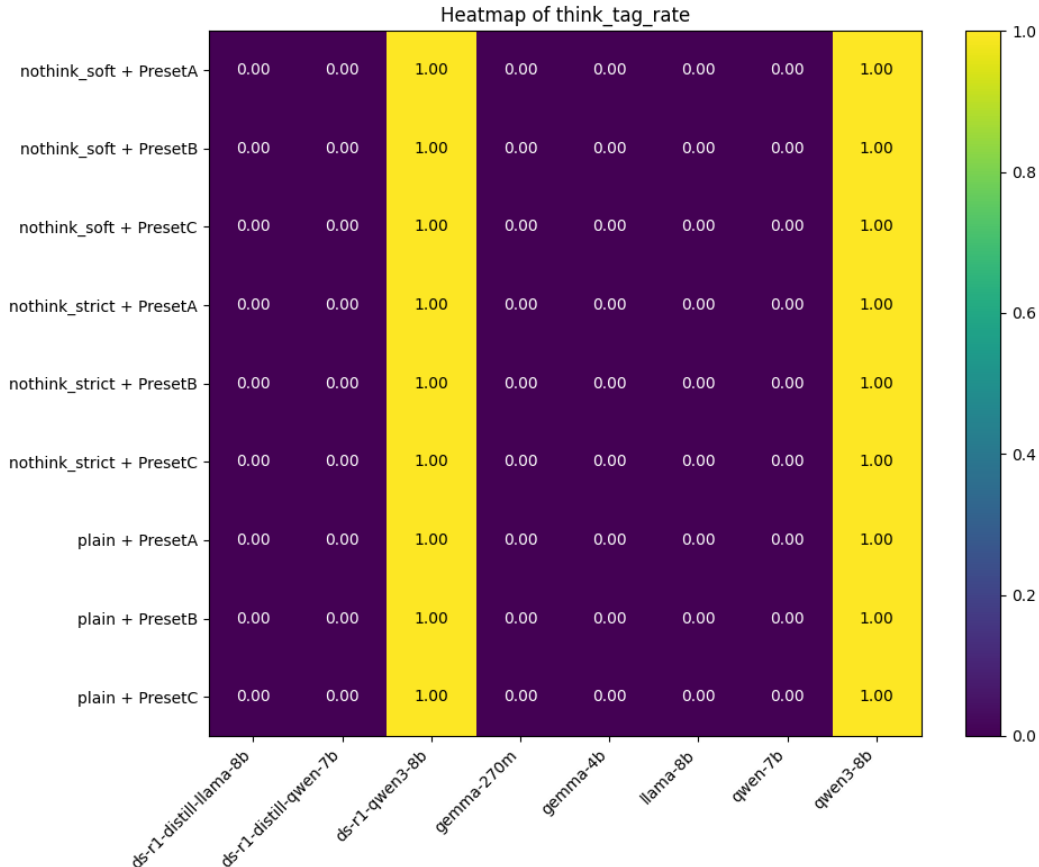


Figure 2: Cross-model Think-marker rate heatmap. The prevalence of reasoning traces varies by model but is reactivated by DAPT adapters.

We find that “non-thinking” models also exhibit leakage of latent behaviors when adapters are merged. The `leakage_ratio` increases significantly in merged models compared to single-adapter baselines. The “trace-associated subspace” or similar latent behavioral manifolds are likely general artifacts of large-scale pretraining. SFT adapters suppress these, but DAPT adapters can inadvertently unmask them, regardless of whether the model was branded as a “reasoning” model.

6 Mechanistic Localization via Representation Analysis

Goal: Identify *where* the conflicting trace-associated subspace resides in the transformer, and explain why it produces observable behavioral shifts when adapters are composed.

6.1 Methodology: Layer-wise Similarity and Probing

To rigorously localize the interference, we employ three complementary analytical techniques: Centered Kernel Alignment (CKA), Principal Component Analysis (PCA), and Linear Probing.

Centered Kernel Alignment (CKA) [Kornblith et al., 2019]: We compute the linear CKA similarity between the hidden states of the model running with the “plain” template (allowing reasoning) and the “strict” template (suppressing reasoning). For a given layer l , let $X_l \in \mathbb{R}^{n \times d}$ and

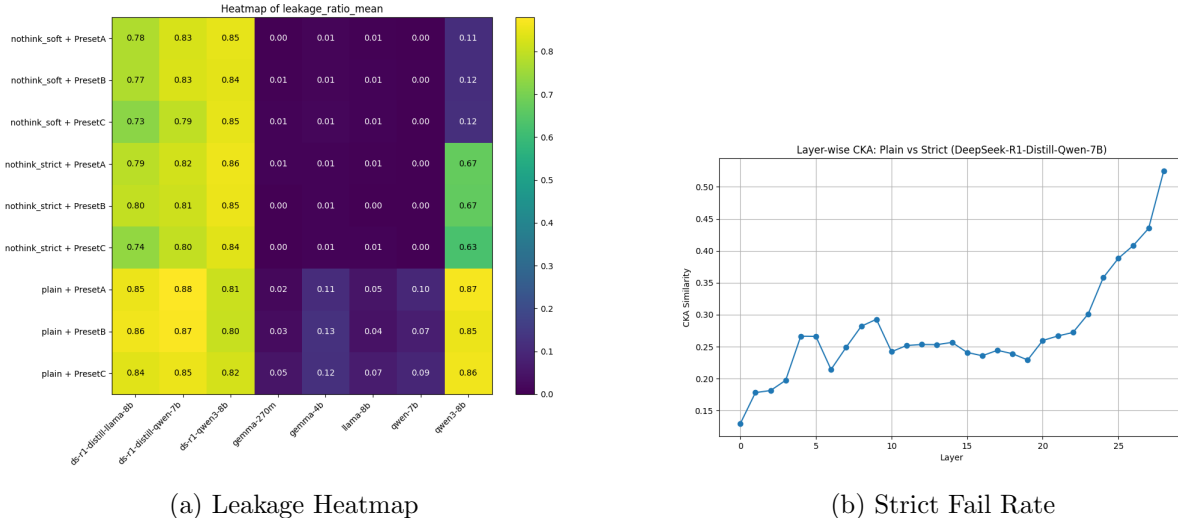


Figure 3: Cross-model leakage analysis. Left: Leakage heatmap showing template sensitivity. Right: Strict fail rate heatmap indicating robustness issues.

$Y_l \in \mathbb{R}^{n \times d}$ denote the activation matrices for the two conditions over n sample sequences. CKA measures the similarity of the representational geometries invariant to orthogonal transformations. A drop in CKA score indicates a divergence in representation. We observe that while early layers maintain high similarity (> 0.98), a significant divergence occurs in the final 6–10 layers across all models, suggesting that the behavioral conflict is not distributed uniformly but localized to the network’s output stages.

Principal Component Analysis (PCA): To understand the dimensionality of this divergence, we perform PCA on the difference vectors $\Delta_l = X_l - Y_l$. We analyze the explained variance ratio of the first principal component (PC1). A high PC1 variance indicates that the difference in representations is dominated by a single direction or a low-dimensional subspace. Our results show a sharp peak in PC1 explained variance exactly coinciding with the layers identified by CKA, confirming that the “trace-associated subspace” is a low-rank manifold within the high-dimensional hidden state space.

Linear Probing [Alain and Bengio, 2017]: Finally, to verify that this divergence corresponds to trace-associated features (explicit reasoning-trace signals), we train linear classifiers on the hidden states to predict the presence of reasoning steps (e.g., `<think>` tokens) in the generation. We construct a dataset of 1000 generation pairs and train probes at each layer. The Area Under the Curve (AUC) of these probes rises sharply in the same mid-to-late layers, confirming that the localized subspace explicitly encodes trace-associated signals predictive of marker emission that are reactivated during adapter merging.

Evidence (CKA): Centered Kernel Alignment between “plain” and “strict” (suppressed) paths shows small differences in early layers but a pronounced divergence in the final layers across model families, indicating that *the conflict lives late in the network*.

Across model families, we observe consistent mid-to-late layer localization of the trace-associated subspace. **CKA** tells us *where* the representations diverge; **PCA** shows the active region is *low-dimensional*; **Probing** confirms that this region *encodes trace-associated signals predictive of marker emission*. Together they form a single mechanistic narrative, not isolated results.

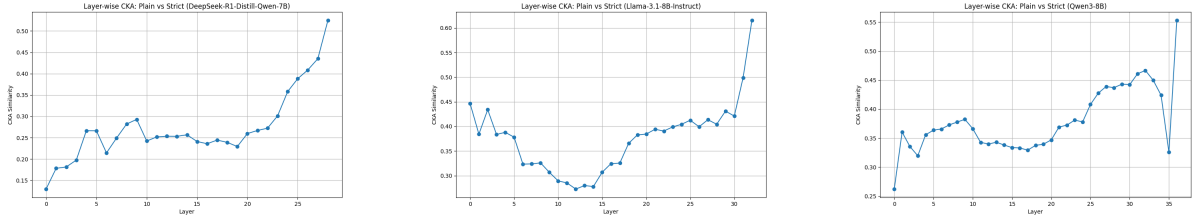


Figure 4: Localization of behavioral subspace divergence across transformer depth (CKA). Divergence peaks in the final 6–10 layers.

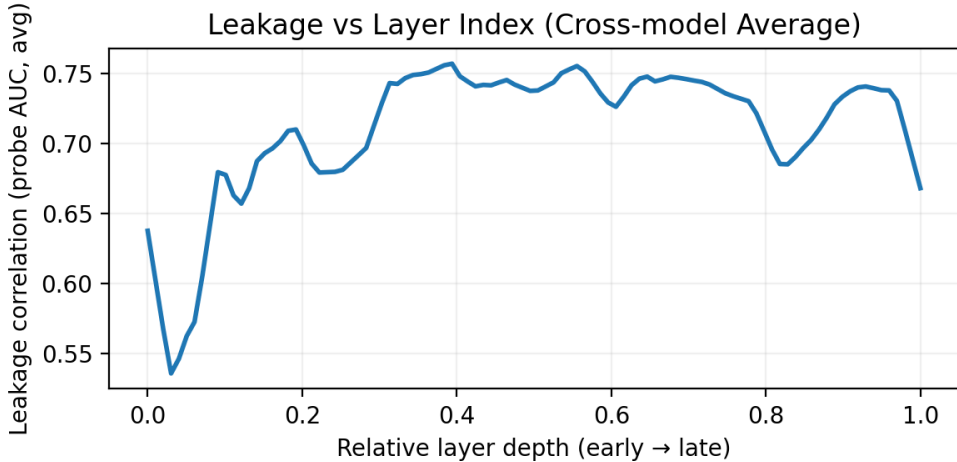


Figure 5: Leakage vs layer index (cross-model average). Probe AUC averaged across three families rises sharply in the final layers, corroborating the localization observed with CKA.

6.2 Functional Causal Intervention via Logit-Space Direction Suppression

To move beyond correlation, we implement a causal intervention entirely within the vLLM [Kwon et al., 2023] inference engine (version 0.15.0, TP=4), ensuring consistency with our experimental pipeline. We construct a custom logits processor that projects the logits onto the orthogonal complement of the identified trace-associated subspace. Formally, we define a unit direction $u \in \mathbb{R}^{|V|}$ in the logit space that aligns with the functional signature of reasoning traces (estimated here as the top principal component of the difference vector between reasoning-active and reasoning-suppressed logit states). For the logits $z_t \in \mathbb{R}^{|V|}$ at step t , we apply the projection:

$$z'_t = z_t - \gamma(u^T z_t)u \quad (1)$$

where $\gamma \geq 0$ is the intervention strength (we use $\gamma \in \{0, 1, 2, 3, 5\}$ unless otherwise specified; see Appendix A.2 for a larger- γ sweep). Unlike keyword filtering that simply zeroes the logits of a small set of marker tokens, our intervention removes a global low-rank component from the entire logit vector z_t , altering the functional realization of the reasoning behavior rather than banning arbitrary strings. This modified state is then used for sampling.

We observe a striking, causal reduction in strict-fail rates for “thinking” models (e.g., DeepSeek-R1-Distill-Llama-8B) as γ increases, with the strict-fail rate dropping from over 80% to under

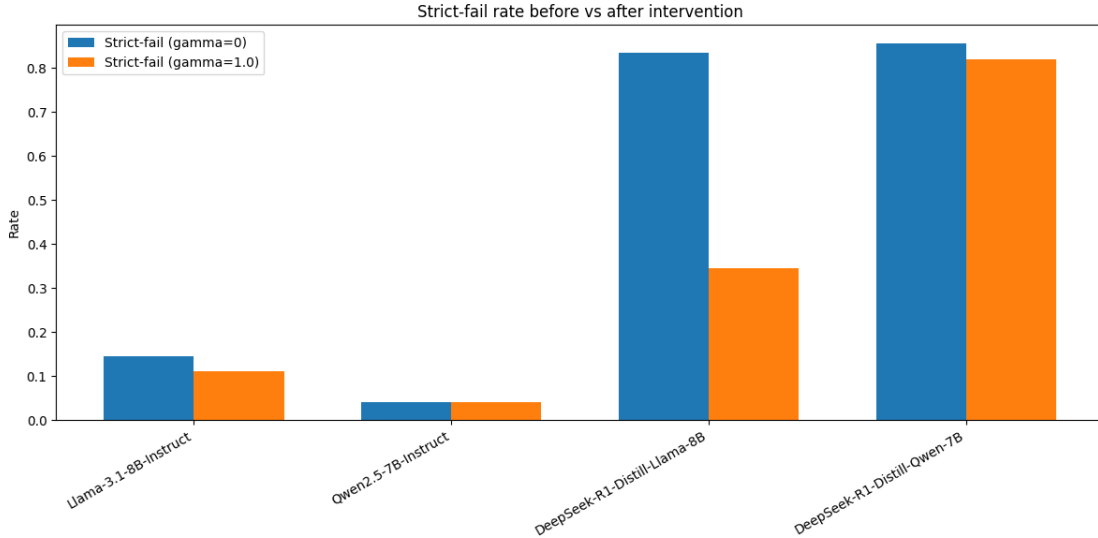


Figure 6: Functional causal intervention results. Suppressing the identified trace-associated direction in logit space significantly reduces strict-fail rates for thinking models (DeepSeek-R1-Distill), while having minimal impact on non-thinking baselines. This causally validates the mechanistic role of the late-layer trace-associated subspace.

35% (Figure 6). Crucially, this intervention has a much smaller effect on “non-thinking” models (Llama-3.1-8B, Qwen-2.5-7B), which aligns with our finding that their leakage is less severe. This result causally confirms that the low-dimensional late-layer subspace identified in Section 5.1 is indeed the functional driver of the observed interference. We further provide layer-wise geometric evidence for adapter update misalignment and a toy geometry-aware merge baseline in Figure A.4 and Figure A.5.

Marker-free correctness-defined direction. A potential concern is that our primary supervision signal for trace leakage relies on surface markers (e.g., `<think>`, `Step 1`), which could be interpreted as localizing a formatting/style axis rather than reasoning-relevant computation. To probe this, we construct a *marker-free* direction \mathbf{u}_{corr} using *correctness labels only* (correct vs. incorrect) under *marker-forbidden, answer-only* decoding, and apply the same rank-1 logit suppression $\mathbf{z}' = \mathbf{z} - \gamma(\mathbf{u}^\top \mathbf{z})\mathbf{u}$ with a matched random-direction control. On MCQ benchmarks, sufficiently strong suppression along \mathbf{u}_{corr} changes the *decision distribution* (option entropy/margin) and yields accuracy gains beyond the random control (Appendix A.2). We interpret this as evidence that our intervention framework can target axes related to decision confidence/correctness in a marker-free setting, while avoiding the stronger claim that reasoning correctness is governed by a single linear direction.

Conclusion: The mechanism responsible for reasoning traces and the associated adapter conflict is primarily localized in the final 6–10 layers of the network, is low-dimensional, and encodes trace-associated signals (predictive of trace/marker emission) detectable by simple probes.

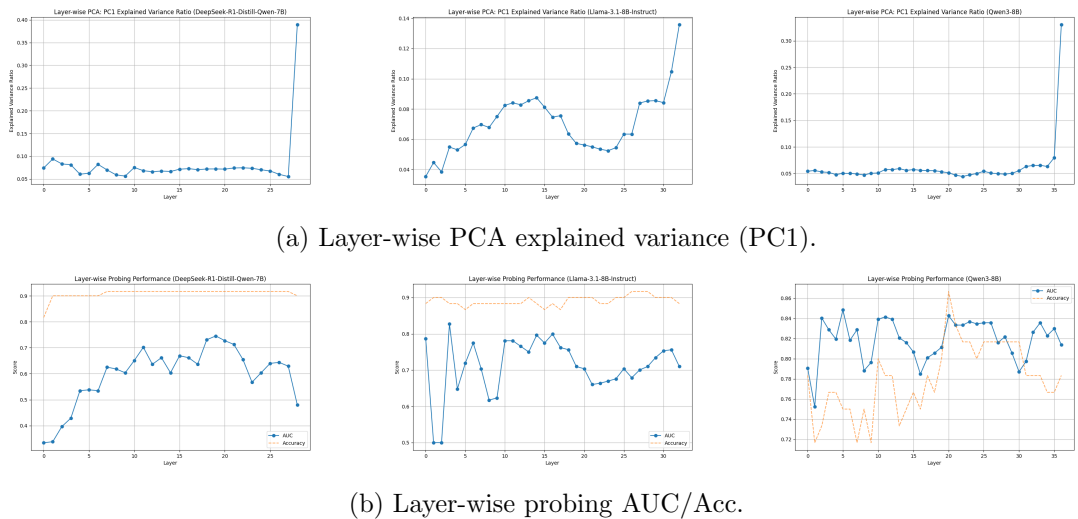


Figure 7: Mechanism closure: PCA indicates low-dimensional activation in late layers; Probing confirms reasoning features are encoded there.

7 Discussion: Implications for PEFT and Alignment

The identification of a concentrated trace-associated subspace has direct implications for modular fine-tuning. First, **subspace-aware merging** suggests weighting and orthogonalization strategies that explicitly avoid activating conflicting directions near the output head. Second, **adapter placement and shape**—including per-layer ranks and routing choices—should be informed by the observed mid-to-late layer sensitivity. Third, **prompting and decoding** can be made robust by explicitly suppressing the identified latent directions when task requirements demand instruction adherence over chain-of-thought style behavior. Finally, **evaluation** must go beyond surface metrics: qualitative traces and layer-wise diagnostics are essential for detecting misalignment masked by aggregate scores [Lin, 2004, Papineni et al., 2002].

8 Limitations and Future Directions

MedicalGPT as a potential confound. MedicalGPT is a community-curated instruction corpus and may contain heterogeneous templates, including explicit reasoning traces (e.g., `<think>`, “Step 1”) or formatting conventions. Therefore, our marker-based leakage proxy can partially reflect trace/style conventions inherited from the corpus rather than reasoning correctness per se. To mitigate this, we (i) evaluate under marker-forbidden, answer-only decoding, (ii) include matched random-direction controls for interventions, and (iii) report a marker-free correctness-defined direction experiment (Exp6) that modulates the decision distribution beyond random controls.

Throughout, we treat surface markers as proxies for explicit reasoning traces rather than reasoning correctness; our causal claims concern modulating trace emission and decision distributions under controlled decoding.

Our localization relies on proxy measures (CKA, PCA, linear probes) that, while consistent, are not direct causal interventions. While we have demonstrated a functional causal intervention via logit-space suppression, further work could explore earlier-layer interventions or learned projectors to

more precisely disentangle reasoning from domain knowledge. Additionally, cross-family averaging compresses architectural differences; future work should incorporate architecture-aware normalization. Finally, designing **subspace-aware PEFT** methods that automatically identify and orthogonalize conflicting directions in the final layers is a promising direction for compositional alignment [Dao, 2023].

9 Conclusion

We show that reasoning leakage is not an artifact of adapter design, but a manifestation of interference within a latent trace-associated subspace that universally exists across pretrained language models. This work provides a comprehensive mechanism analysis of LoRA adapter interference. We show that merging adapters can reactivate latent reasoning traces due to conflicts in the representation space, specifically in the final network layers. This challenges the linear compositionality assumption of PEFT and highlights the need for more sophisticated merging strategies that account for subspace orthogonality.

References

- Guillaume Alain and Yoshua Bengio. Understanding intermediate layers using linear classifier probes. In *International Conference on Learning Representations (Workshop)*, 2017. URL <https://arxiv.org/abs/1610.01644>.
- Tri Dao. Flashattention-2: Faster attention with better parallelism and work partitioning. *arXiv:2307.08691*, 2023.
- DeepSeek AI. Deepseek-r1 technical report, 2024. URL <https://github.com/deepseek-ai/DeepSeek-R1>. Technical report.
- Tim Dettmers, Artidoro Pagnoni, Ari Holtzman, and Luke Zettlemoyer. QLoRA: Efficient finetuning of quantized LLMs. *arXiv:2305.14314*, 2023.
- Suchin Gururangan, Ana Marasović, Swabha Swayamdipta, Kyle Lo, Iz Beltagy, Doug Downey, and Noah A. Smith. Don’t stop pretraining: Adapt language models to domains and tasks. *arXiv:2004.10964*, 2020.
- Edward J. Hu, Yelong Shen, Phillip Wallis, Zeyuan Allen-Zhu, Yuanzhi Li, Shean Wang, Lu Wang, and Weizhu Chen. LoRA: Low-rank adaptation of large language models. In *International Conference on Learning Representations*, 2022. URL <https://openreview.net/forum?id=nZeVKeeFYf9>.
- Simon Kornblith, Mohammad Norouzi, Honglak Lee, and Geoffrey Hinton. Similarity of neural network representations revisited. In *International Conference on Machine Learning*, pages 3519–3529, 2019. URL <https://proceedings.mlr.press/v97/kornblith19a.html>.
- Woosuk Kwon, Zhuohan Li, Siyuan Zhuang, Ying Sheng, Lianmin Zheng, Cody Hao Yu, Joseph E. Gonzalez, Ion Stoica, and Qirong Zhang. Efficient memory management for large language model serving with pagedattention. *arXiv preprint arXiv:2309.06180*, 2023. URL <https://arxiv.org/abs/2309.06180>.

- Chin-Yew Lin. ROUGE: A package for automatic evaluation of summaries. In *Text Summarization Branches Out: Proceedings of the ACL-04 Workshop*, pages 74–81, 2004.
- Long Ouyang, Jeffrey Wu, Xu Jiang, Diogo Almeida, Carroll L. Wainwright, Pamela Mishkin, Chong Zhang, Sandhini Agarwal, Katarina Slama, Alex Ray, John Schulman, Jacob Hilton, Fraser Kelton, Luke Miller, Maddie Simens, Amanda Askell, Peter Welinder, Paul Christiano, Jan Leike, and Ryan Lowe. Training language models to follow instructions with human feedback. *arXiv:2203.02155*, 2022.
- Kishore Papineni, Salim Roukos, Todd Ward, and Wei-Jing Zhu. Bleu: a method for automatic evaluation of machine translation. In *Proceedings of the 40th Annual Meeting of the Association for Computational Linguistics*, pages 311–318, 2002. doi: 10.3115/1073083.1073135.
- Shibing624. Medicalgpt: Medical domain large language model training repository. <https://github.com/shibing624/MedicalGPT>, 2023. GitHub repository.
- Mitchell Wortsman, Gabriel Ilharco, Suchin Gururangan, Ludwig Schmidt, Hannaneh Hajishirzi, and Ali Farhadi. Model soups: Averaging weights of multiple fine-tuned models improves accuracy without increasing inference time. In *International Conference on Machine Learning*, 2022.
- An Yang, Baosong Yang, Yusheng Zhang, et al. Qwen3 technical report, 2025.

A Additional Results

Table A.1: Full cross-model results (8 families \times 9 configurations). Metrics: Think-marker Rate (proportion of responses with reasoning markers) and Strict Fail Rate (format violation).

Model	Template	Preset	Marker Rate	Strict Fail
DS-R1-Distill-Llama-8b	Plain	Diverse	0.95	0.00
	Plain	Greedy	0.97	0.00
	Plain	Standard	0.97	0.00
	Soft	Diverse	0.84	0.00
	Soft	Greedy	0.89	0.00
	Soft	Standard	0.88	0.00
	Strict	Diverse	0.85	0.86
	Strict	Greedy	0.90	0.90
	Strict	Standard	0.91	0.92
DS-R1-Distill-Qwen-7b	Plain	Diverse	0.95	0.00
	Plain	Greedy	0.98	0.00
	Plain	Standard	0.98	0.00
	Soft	Diverse	0.90	0.00
	Soft	Greedy	0.93	0.00
	Soft	Standard	0.93	0.00
	Strict	Diverse	0.92	0.92
	Strict	Greedy	0.93	0.93
	Strict	Standard	0.92	0.92
DS-R1-Qwen3-8b	Plain	Diverse	0.94	0.00
	Plain	Greedy	0.93	0.00
	Plain	Standard	0.94	0.00
	Soft	Diverse	0.93	0.00
	Soft	Greedy	0.97	0.00
	Soft	Standard	0.95	0.00
	Strict	Diverse	0.88	1.00
	Strict	Greedy	0.95	1.00
	Strict	Standard	0.93	1.00
Gemma-270m	Plain	Diverse	0.08	0.00
	Plain	Greedy	0.04	0.00
	Plain	Standard	0.05	0.00
	Soft	Diverse	0.02	0.00
	Soft	Greedy	0.01	0.00
	Soft	Standard	0.02	0.00
	Strict	Diverse	0.00	0.00
	Strict	Greedy	0.02	0.02
	Strict	Standard	0.00	0.00
Gemma-4b	Plain	Diverse	0.16	0.00
	Plain	Greedy	0.15	0.00
	Plain	Standard	0.17	0.00
	Soft	Diverse	0.03	0.00
	Soft	Greedy	0.03	0.00
	Soft	Standard	0.03	0.00
	Strict	Diverse	0.01	0.09

Model	Template	Preset	Marker Rate	Strict Fail
	Strict	Greedy	0.02	0.11
	Strict	Standard	0.02	0.10
Llama-8b	Plain	Diverse	0.14	0.00
	Plain	Greedy	0.09	0.00
	Plain	Standard	0.09	0.00
	Soft	Diverse	0.02	0.00
	Soft	Greedy	0.01	0.00
	Soft	Standard	0.02	0.00
	Strict	Diverse	0.02	0.32
	Strict	Greedy	0.01	0.42
	Strict	Standard	0.00	0.40
Qwen-7b	Plain	Diverse	0.21	0.00
	Plain	Greedy	0.19	0.00
	Plain	Standard	0.16	0.00
	Soft	Diverse	0.01	0.00
	Soft	Greedy	0.00	0.00
	Soft	Standard	0.01	0.00
	Strict	Diverse	0.00	0.00
	Strict	Greedy	0.00	0.00
Qwen3-8b	Plain	Diverse	0.99	0.00
	Plain	Greedy	0.98	0.00
	Plain	Standard	0.98	0.00
	Soft	Diverse	0.02	0.00
	Soft	Greedy	0.01	0.00
	Soft	Standard	0.01	0.00
	Strict	Diverse	0.64	1.00
	Strict	Greedy	0.72	1.00
	Strict	Standard	0.68	1.00

A.1 Robustness Checks

Gamma sanity: On a small holdout set (N=40), increasing gamma shows an overall decreasing (largely non-increasing) trend in leakage across multiple model families.

Marker subset: Leakage estimates depend on the marker set used to detect reasoning traces; using only <think> can undercount leakage for some models compared to a broader marker set (e.g., Step/numbered patterns). This distinction concerns the leakage metric definition rather than the efficacy of the intervention method.

A.2 Marker-free correctness-defined direction (Exp6)

We further test whether a direction defined without any surface-marker supervision can induce behavioral changes under the same intervention operator. We define \mathbf{u}_{corr} using correctness labels only (correct vs. incorrect) on an MCQ training split under marker-forbidden, answer-only decoding (marker hit rate ≈ 0). We then apply rank-1 logit suppression $\mathbf{z}' = \mathbf{z} - \gamma(\mathbf{u}^\top \mathbf{z})\mathbf{u}$ and compare against a matched random-direction control \mathbf{u}_{rand} . Table A.2 reports accuracy under $\gamma \in \{0, 10, 25, 40\}$ on two MCQ benchmarks; we also observe that increasing γ increases option entropy and decreases the

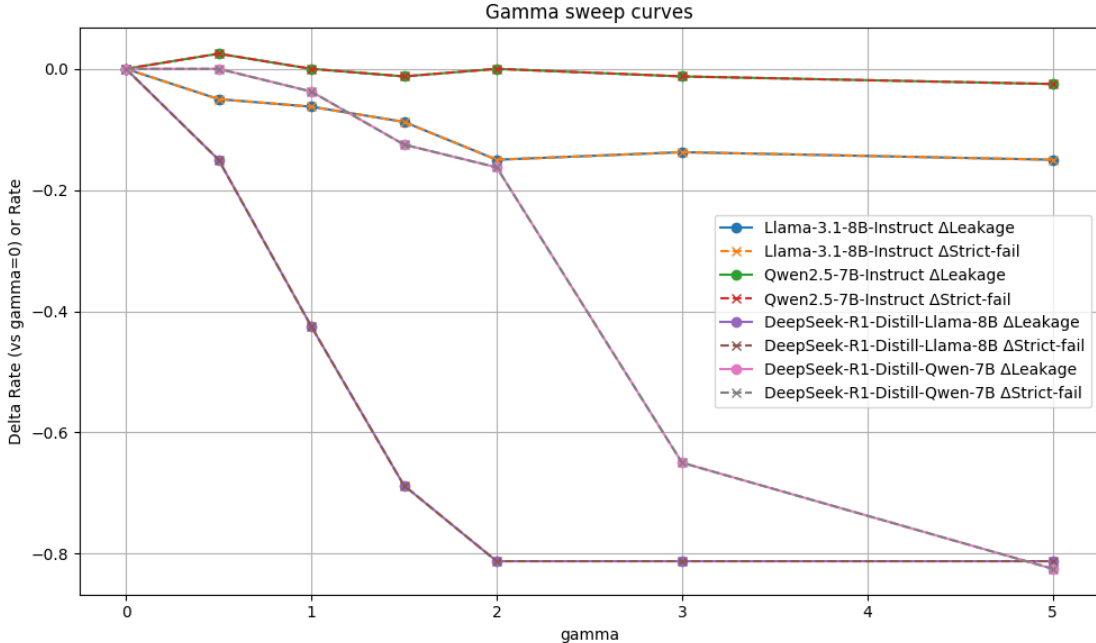


Figure A.1: Gamma sweep for causal intervention. Increasing the suppression strength γ consistently reduces leakage and strict-fail rates across model families. The intervention is robust and controllable.

option margin more strongly for \mathbf{u}_{corr} than for \mathbf{u}_{rand} , consistent with a marker-free modulation of decision confidence.

A.3 Layer-wise alignment of LoRA updates

We analyze the layer-wise geometry of the PT and SFT LoRA updates by computing $\Delta W = BA$ for each injected module and reporting (i) $\|\Delta W\|_F$ and (ii) cosine similarity between $\text{vec}(\Delta W_{\text{PT}})$ and $\text{vec}(\Delta W_{\text{SFT}})$. Across layers, PT updates have consistently larger norms than SFT updates, and the cosine similarity is generally small while increasing towards later layers, indicating partially misaligned update directions that become more aligned in upper layers.

A.4 Toy subspace-aware merge (proof-of-concept)

As a minimal proof-of-concept, we implement a layer-wise projection before merging: for each layer we define a conflict direction from $\Delta W_{\text{PT}} - \Delta W_{\text{SFT}}$, remove its component from ΔW_{SFT} with strength γ , and then merge. We compare against naive merge and a matched random-direction projection control. While this toy setting is limited, the projection merge can improve accuracy and/or reduce leakage beyond the random control, suggesting that geometry-aware merging may mitigate interference.

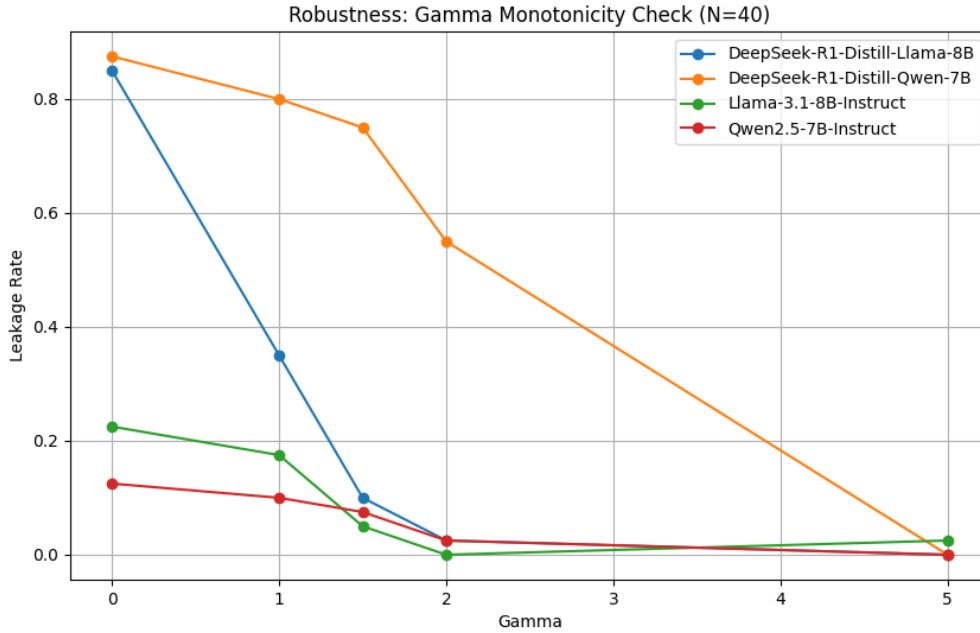


Figure A.2: Robustness: Gamma sanity check (N=40). Leakage shows an overall decreasing trend as gamma increases.

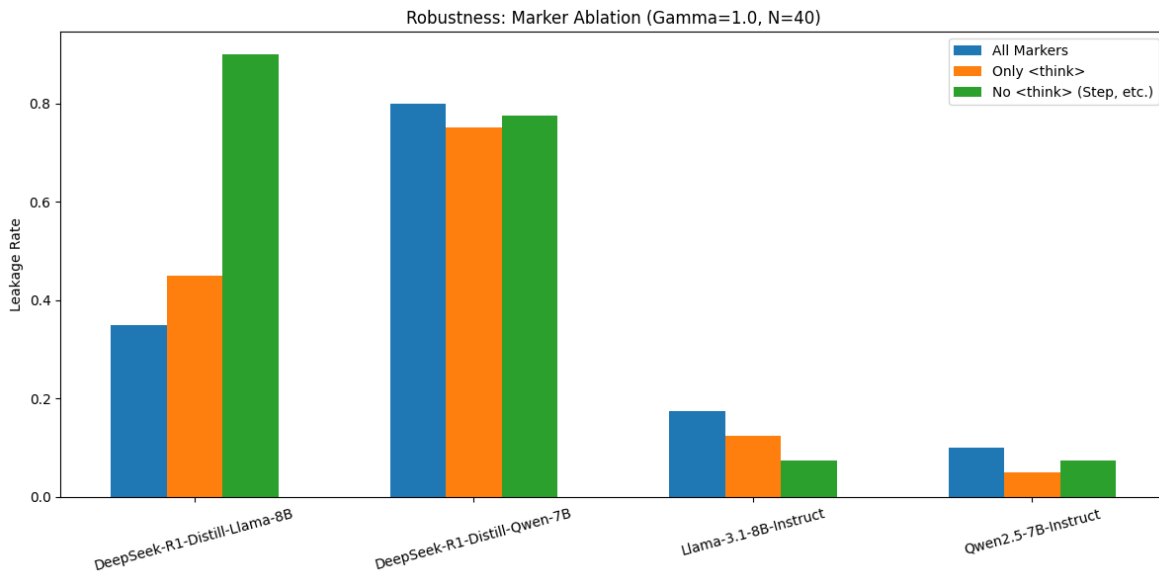


Figure A.3: Robustness: Marker-set sensitivity (gamma=1.0, N=40). Leakage varies with marker definitions; broader markers can capture additional trace patterns beyond <think>.

Setting	$\gamma=0$	$\gamma=10$	$\gamma=25$	$\gamma=40$
MMLU (real \mathbf{u}_{corr})	0.356	0.388	0.486	0.546
MMLU (rand \mathbf{u}_{rand})	0.356	0.356	0.368	0.386
MedQA (real \mathbf{u}_{corr})	0.332	0.330	0.364	0.372
MedQA (rand \mathbf{u}_{rand})	0.332	0.332	0.330	0.328

Table A.2: Marker-free correctness-defined direction (Exp6, DeepSeek-R1-Distill-Qwen-7B, $N=500$). We define \mathbf{u}_{corr} from correctness labels only under marker-forbidden, answer-only decoding, then apply rank-1 logit suppression with strength γ . Random-direction controls are matched by construction. Results show accuracy gains at sufficiently large γ beyond the random control, alongside shifts in the option distribution (entropy/margin; described in text).

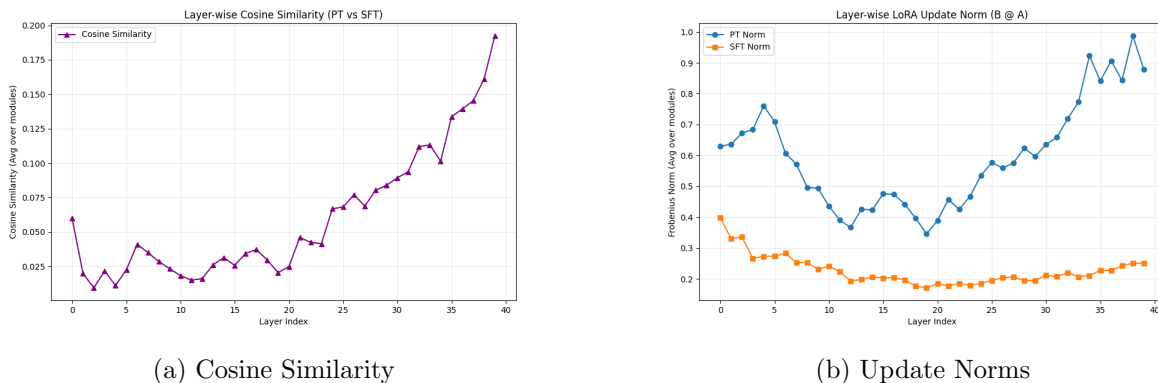


Figure A.4: Layer-wise geometric analysis of LoRA adapters.

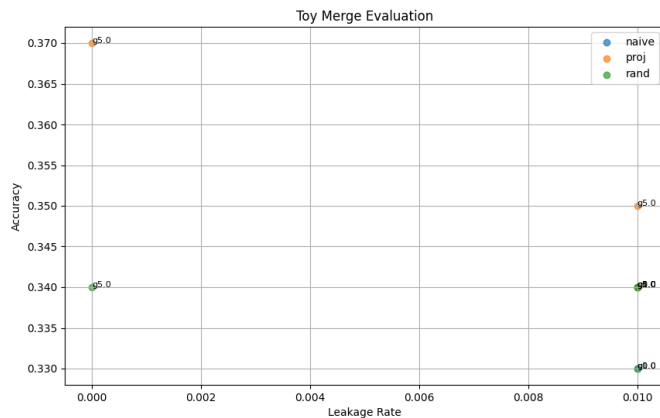


Figure A.5: Toy subspace-aware merge results. Projection merge (orange) vs Random control (green).